Solid Oxide Cell Systems for Polygeneration Purposes

Rokni, Masoud

Publication date:
2018

Document Version
Publisher's PDF, also known as Version of record

Proceedings of the 3rs South East European Conference on Sustainable Development of Energy, Water and Environment Systems *SEE SDEWES 2018,* June 30 -July 4, Novi Sad, Serbia. Paper nr. 0120

Solid Oxide Cell Systems for Polygeneration Purposes

M. Rokni*
Technical University of Denmark, Department of Mechanical Engineering, Thermal Energy
Copenhagen, Denmark
e–mail: MR@mek.dtu.dk

ABSTRACT

A novel plant based on reversible solid oxide cell, absorption chiller, water distillation and wind turbines is designed and analysed. The main goal is produce hydrogen from excess electricity generated by the wind turbines. The off-heat from the plant is recovered to generate heat, cool or freshwater. Thus, different plant designs are presented depending on the demand and location. Further, solar energy is used to heat up water and regulate the heat production for the district heating. It is shown that the plant is able to produce hydrogen at about 2000 kg/day and the plant hydrogen production efficiency reaches to about 44%. Total plant efficiency (energy efficiency) will be close to 52% when heat, cool and freshwater are accounted. Neglecting the heat input through solar energy to the system, then hydrogen production efficiency will be about 75% and the total plant efficiency will be about 90%. In addition, plant performance versus wind velocity is also analysed in terms of heating, cooling and freshwater generation.

KEYWORDS

SOC, polygeneration, DCMD, chiller, freshwater, solar energy.

INTRODUCTION

Owing to global warming and its consequences, renewable energy production technologies will be called to play a significant role in the immediate future. Therefore, it is essential to find new, effective solutions that allow for the integration of sustainable energy production techniques into the current existing systems and thereby decreasing the emissions. In order to use the most energy of the renewable sources then it is key that these such solutions are can be used for polygenerations purposes such as electricity, fuel and freshwater production (instead of dissipating heat to the environment).

Electrolysis technology such as solid oxide electrolyte cell (SOEC) can be used to store the excess energy in fuel form when the renewable source is high enough. The stored fuel can then be used to generate heat/cool, power and freshwater by a solid oxide fuel cell (SOFC) when the renewable source is low, such as during night time when using sun energy or on a calm day when using wind energy. This implies that there is a need for a reversible solid oxide cell (RSOC) that can produce synthetic fuel from electricity, or produce electricity from fuel when reversed.

Several studies on SOEC systems have been conducted; for example, [1] reviewed technological development of hydrogen production from an SOEC system in terms of materials, cell configuration designs, electrode depolarizations and mathematical modelling. [2] presented the exergoeconomic analysis of a hybrid system based on steam biomass gasification for

* Corresponding author

hydrogen production. [3] showed the feasibility of the concept and successful reversible operation of a dual cell through electrochemical tests carried out by impedance spectroscopy. [4] carried out an experimental study to demonstrate the heat spreading capabilities and power limitations of high-temperature applications in SOEC/SOFC stacks

Direct contact membrane distillation (DCMD) is a thermal separation process where only the water vapour (or other volatile) passes through a micro-porous hydrophobic membrane while impurities, such as salt, cannot cross the membrane. The vapour pressure gradient created by the temperature difference between both sides of the membrane drives the process. [5] reviewed the desalination of seawater by the DCMD system, and its performance from laboratory scale to pilot projects. [6] showed experimentally that 99.99% of salt can be separated from hot water at 80°C in optimum conditions and with optimum membrane material selection. Desalination powered by solar energy is an attractive solution that can address the worldwide water-shortage problem without contributing significantly to greenhouse gas emissions. It is worth noting that often there is shortage of fresh water where solar radiation is high. As deliberated in [7], a promising system for renewable energy desalination is the utilization of low-temperature DCMD systems. The study by [8] showed that experimental data agreed very well with the calculated results in terms of vapour mass flux, as well as membrane and total heat transfer coefficients. In addition, such a technique has a great advantage because it works at lower temperatures, even down to 40°C, which allows it to use lower temperatures sources and avoid the great latent heat of water [9].

In this work, a poly-generation system is presented that uses wind turbines to convert wind energy into electricity and drive a RSOC. Further, the waste heat is recovered for seawater distillation through a DCMD technique and/or to produce heat/cool for district heating/cooling system. Such a system will result in flexible poly-generation plant driven by wind energy that can be regulated for different output combinations of hydrogen, electricity, heat/cool and freshwater. A complete balance of plant is first designed, and then alternative system designs will be presented. The performance of each design is then analysed thermodynamically.

To the best of the author's knowledge, no similar studies exist in the open literature. Therefore, this study may provide some inspiration for further analysis and perhaps implementation of such technology into current existing systems. The objective of the present is not to study the cost associated with the system but present an attractive system, which might be of interest for the future power generations.

MODELLING OF DIFFERENT COMPONENTS

RSOC modelling

This model is based on the model presented by [10] and [11], which also contain a detailed electrochemical model, and captures the experimental data very well. First, pressures at the gas outlets are simply calculated using the input parameters as follows:

$$p_{ca_{out}} = p_{ca_{in}} - dp_{ca} \quad (1)$$

$$p_{an\_out} = p_{an_{in}} - dp_{an} \quad (2)$$

where dp_{ca} and dp_{an} are the relative pressure drops at the anode and cathode sides, respectively. Then, the cell voltage and the current density are calculated using the power input

$$P_{SOEC} = N_{stack} N_{cell} E_{cell} A_{cell} J \quad (3)$$

where N_{stack}, N_{cell}, E_{cell}, A_{cell} and J are the number of stacks, number of cells per stack, cell voltage, single cell area and current density, respectively. The Nernst potential gives the theoretical minimum electrical work, but in reality, part of the voltage is lost irreversibly owing to polarizations such as ohmic, activation, and concentration polarizations. The cell voltage can be calculated by following equation:

$$E_{cell} = E_{Nernst} + \Delta E_{act} + \Delta E_{ohm} + \Delta E_{conc} \quad (4)$$

where the cell voltage is calculated by adding the polarizations (activation, ohmic and concentration) to the Nernst voltage. Each polarization is then carefully modelled. The ohmic resistance remains constant while the other two vary depending on the current applied, i.e., ohmic polarization increases proportionally with the current, while activation polarization and concentration polarization are dominant at low and high current levels, respectively [12]. Thus, the minimum electrical work that has to be applied to the RSOC is determined by the Nernst potential plus the polarization losses.

The Nernst potential and the polarizations in the RSOC (activation, ohmic and concentration) are calculated as explained in [12] and [11]. The diffusion coefficient is approximated using the kinetic theory and the Chapman–Enskog theory [13]. Note that the energy applied through electrical work might not be enough to drive the system's unspontaneous reactions. The remaining energy is then applied by a heat source at higher temperature and/or by directly increasing the power (increasing the current through the cells), which in turn produces more heat owing to the Joule effect [14]. When the heat produced equals the heat demand in the reaction (thermo-neutral point), then the voltage becomes

$$E_{tnp} = \frac{\Delta_r H}{2F} \quad (5)$$

where $\Delta_r H$ is the enthalpy change in the reactions, and F is the Faraday constant (96485.34 C/mol). The outlet concentrations and mass flows can be determined by molar balance of each element and using the current density to determine the quantity of reactions taking place. The molar production of *H2* (or moles of *H2O* molecules split) is fixed for a certain current value; consequently, *O2* is produced according to the reaction

$$\dot{m}_{H2,out} = \frac{N_{stack} N_{cell} A_{cell} J}{2F} \quad (6)$$

$$\dot{m}_{H2O,out} = \dot{m}_{H2O,in} - \dot{m}_{H2O,split} = \dot{m}_{H2O,in} - \frac{N_{stack} N_{cell} A_{cell} J}{2F} \quad (7)$$

$$\dot{m}_{O2,out} = \dot{m}_{O2,in} - \frac{\dot{m}_{H2O,split}}{2} = \dot{m}_{H2O,in} - \frac{N_{stack} N_{cell} A_{cell} J}{4F} \quad (8)$$

The power, the voltage and the current are dependent on each other; therefore, if one of them is defined, the others can be determined. Another way of defining these parameters would be by fixing the H2 production or fixing the molar fraction at the outlet. Finally, the efficiency is defined as

$$\eta_{SOEC} = \frac{\dot{m}_{H2,out} LHV_{H2}}{P_{in} + Q_{in}} \quad (9)$$

where P_{in} and Q_{in} are the electrical power required to run the electrolyzer and the heat input required to preheat the water, while $\dot{m}_{H2,out}$ is the mass flow rate of hydrogen production and

LHV_{H2} is the lower heating value of the hydrogen.

[11] and [12] discussed the validity of the model with experimental data in terms of energy efficiency and *H2O* conversion for different current densities and at different operating temperatures. Table 2 illustrates the main parameters for the RSOC component.

Table 1: Specifications for RSOC (anode and cathode referred to fuel cell mode).

Parameter	**Value**
Anode thickness	*600 µm (Nickel and Yttria Stabilized Zirconia cermet)*
Cathode thickness	*50 µm (Strontium-doped lanthanum manganite)*
Electrolyte thickness	*10 µm (Yttria Stabilized Zirconia)*
Cell area	*144 cm2 (12 cm × 12 cm)*
Operating temperature	*750 °C*
Porosity	*30%*
Tortuosity	*2.5*
Nr. of cells per stack	*70*
Number of stacks	*200*

DCMD modelling

For this component, a hollow fibre configuration is chosen, as described in [15]. The warm seawater flows in the fibres (the feed side), while cold water flows through the permeate side, which is located at the other side of the fibres. The design is made in such a way that both sides have a constant flow, see Fig. 1. Owing to the counter-flow configuration, the temperature difference along the fibre is almost constant and therefore is the associated vapour pressure difference. The pressure gradient across the membrane is the force that drives the entire process. The modelling along the fibre is performed by dividing the fibre into smaller segments or volumes of control, and applying the balance equations (mass flow and energy) using the mean properties of the segment and the state of each segment (temperature, density, pressure, etc.). Note that if the system is not discretized, then the non-linear behaviour of the system leads to large errors in the results.

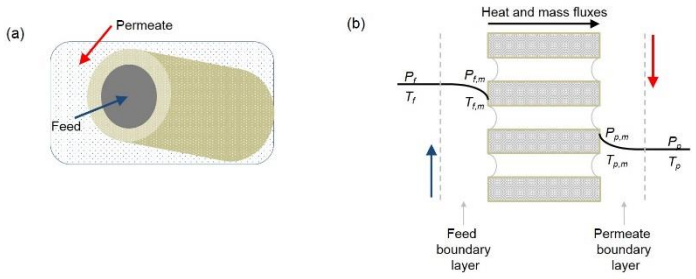

Figure 1: Scheme of (a) cross section of the membrane and (b) the mass and heat transfer through the membrane

The range of operation of the model for the mass flow of one unit is between 0.05–0.15 kg/s; however, higher values can also be applied. In such cases, the model calculates the needed number of units. The range of operation for the feed temperature has limits, and in this study, it is set between 70 °C to 90 °C. The permeate flow is assumed to remain at a constant in-flow of 0.1 kg/s in each unit and at 25°C at the inlet.

Another important issue to consider, when designing the hollow fibre operation, is the

membrane liquid entry pressure (LEP), which sets the limit for the applied transmembrane pressure. Transmembrane pressure is defined as the hydrostatic pressure minus the vapour pressure ($p_{p,m} - p_p$ and $p_f - p_{f,m}$). Values below such limits will prevent liquid from entering the pores. Note that the hydrostatic pressure does not affect the permeate flux, but it is important to consider, as it prevents the pores from flooding. The detailed mathematical model for this component is explained in [16]. Figure 2 shows the DCMD plant while table 2 presents data related to the DCMD used here. The design of freshwater unit is rather simple. Seawater is preheated by freshwater and by a heat source (SwP3 and SwP4 heat exchangers in the figure, respectively) before entering the DCMD. In this study, the heat source is the off-heat after the electrolyser. Note that the freshwater loop is closed loop and is drives by a small water pump. Further, the freshwater will be collected in a tank, while the non-desalinated seawater goes back into the sea again. The slat and other particles that cannot pass though the pores of the DCMD flows along the non-desalinated seawater to the sea. The fibre length, diameter and other parameters are based on the study of [16].

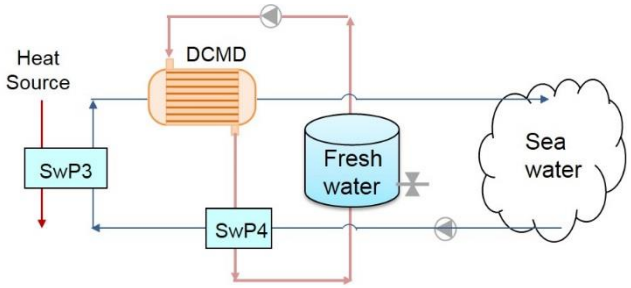

Figure 2: Scheme of a DCMD plant. Seawater preheats by freshwater (SwP4) and then by a heat source (SwP3).

Table 2: DCMD hollow fibre module specifications.

Parameter	Value
Fibre length	*0.4 m*
Inner diameter of fibre	*0.3 mm*
Membrane thickness	*60 μm*
Porosity	*75%*
Membrane conductivity	*0.25 W/mK*
Shell diameter	*0.003 m*
Number of fibres	*3000*
Packing density	*60%*
Inlet temperature	*80 ℃*
Model Constants	
C_k	*15.18 × 10^{-4} [–]*
C_m	*5.1 × 103 m^{-1}*
C_p	*12.97 × 10–11 m*

Absorption chiller modelling

Refrigeration systems based on vapour absorption cycles are a well-known technology, which has extensively been studied for many years [17]. Nevertheless, their market share is still limited compared to the vapour compression systems. The fundamental reasons for this aspect are the relatively low efficiency in delivering cooling needs as well as the high initial capital costs. Regarding the Coefficient Of Performance (COP), which is defined as the ratio between the achieved cooling capacity and the heat input to the cycle. Its value is usually lower than 1

(typically within 0.5 to 0.9), while vapour compression cycles display value higher than 3 based on the electrical input [18] and [19]. Despite their disadvantages, the utilization of absorption cycles is significantly favoured when waste heat is available. More specifically, it is very often the case when hot exhaust gases resulting from industrial processes are released in the surroundings. Thus the integration of absorption chillers, which will utilize this heat that otherwise would be wasted, can lead to an increase in the overall efficiency of the plant.

The driving force of an absorption cycle is a solution consisting of a refrigerant and an absorbent. In most cases the mixture water with lithium-bromide or, water with ammonia is utilized. Furthermore, the cycles can be single, double or triple effect, depending on the available waste heat temperature and the potential investment. In general, multistage cycles need higher temperature heat sources and are characterized by higher values of COP compared to the single stage ones. On the other hand, the installation is more complex since larger number of components will be required which results in higher capital costs [20]. This study uses the mixture of water with lithium-bromide (LiBr) and Fig. 3 shows the absorption plant designed in this study.

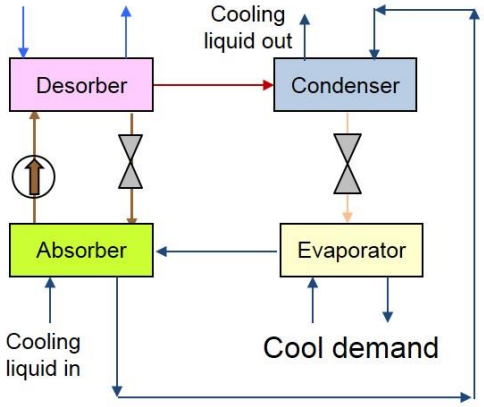

Figure 3: Scheme of the absorption chiller.

In this study, lithium-bromide solution is used by taking into count the properties of this mixture such as enthalpy; entropy and heat capacity are accounted (see e.g. [21]). Table 3 shows parameters used in this study for the absorption chiller.

Table 3: The main parameters for absorption chiller, basic case.

Parameter	Value
Desorber gas outlet temperature	*135 ℃*
Rich solution	*0.593 (–)*
Week solution	*0.548 (–)*
Condenser outlet temperature	*32 ℃*
Rich solution pressure after valve	*0.008 bar*
Absorber cooling inlet temperature	*15 ℃*
Absorber cooling inlet pressure	*16 bar*
Solution pump pressure	*0.05 bar*

Wind turbine modelling

Wind turbines (WT) can be divided into two different designs according to the axis of the main shaft rotation. Hence, WTs are either horizontal axis or vertical axis. Horizontal axis wind

turbines are by far the most used kind and therefore this study focuses on this kind only. Further from an operational point of view, WTs can either works at constant shaft speed or at variable shaft speed. The later has a more complex and expensive design due to their need of some extra components. On the other hand, variable wind turbines can always operate at their peak efficiency for a wide range of wind velocity. The fixed speed ones, instead, are designed to operate at their optimal efficiency only for one value of wind speed, which is statically the most probable for the place of installation.

Due to Betz law the maximum theoretical efficiency of a wind turbine is equal to 16/27 ≈ 0.593. The mechanical power of a WT is calculates as

$$\dot{W}_m = \frac{1}{2}\rho_H S u_w^3 C_p \tag{10}$$

where, ρ_H, S, u_w and C_p are air density at hub height [kg/m^3], the swept area ($S = \pi R^2$), wind speed [m/s] and the so called power coefficient. Air density at hub height is calculated as

$$\rho_H = \rho_o exp\left(\frac{-0.297}{3048H}\right) \tag{11}$$

where ρ_o = 1.225 [kg/m^3] is the air density at sea level. The swept area $S = \pi R^2$[m^2]. The power coefficient is a function of pitch angle θ [°] and the tip speed ratio λ [rad]. The pitch angle allows the blades rotation along their longitudinal axis. λ is defined as

$$\lambda = \frac{w_b R}{u_w} \tag{12}$$

where w_b and R are the the blade angular rotation [rad/s] (rotational speed) and rotor radius [m]. The blade angular rotation is defined as

$$w_b = \frac{2\pi n}{60} \tag{13}$$

where n is the rotor angular velocity [rpm]. The power coefficient is defined as in [22],

$$C_p = C_1\left(\frac{C_2}{\beta} - C_3\beta\theta - C_4\theta - C_5\right) exp\left(\frac{-C_6}{\beta}\right) \tag{14}$$

where C_1 = 0.5, C_2 = 116, C_3 = 0.4, C_4 = 0, C_5 = 5, C_6 = 21 and β is

$$\frac{1}{\beta} = \frac{1}{\lambda + 0.08\theta} - \frac{0.035}{1+\theta^3} \tag{15}$$

The electric power is then calculates as

$$\dot{W}_{el} = N_{WT}\,\eta_{conv}\,\dot{W}_m \tag{16}$$

where η_{conv} is the mechanical to electrical conversion efficiency and N_{WT} is the number of wind turbines in the windfarm.

Electrical power from a wind turbine strongly depends on the wind velocity, rotational speed (blades rpm) and wind direction to the blades (angle of attack).

The power produced by the wind turbines are AC (altering current) while the power feed to the electrolyser is DC (direct current), therefore the design includes an AC/DC converter, which has an efficiency of 0.95 %. Further, WTs can work either at constant shaft speed or at variable shaft speed. The later have a more complex design compared to the former one due to the need for additional components. However, variable shaft speed WTs can work at their peak efficiency for a wide range of wind velocities. Table 4 presents parameters assumed in this study for basic case.

Table 4: Wind turbine model specifications used in this study.

Parameter	Value
Blade radius	*30 m*
Hub height	*100 m*
Rotational speed	*15 rpm*
Angle of attack	*10 °*
Conversion efficiency	*0.85*
Number of wind turbines	*13*
Wind speed (default)	*12 m/s*

Modelling of PTSC (parabolic trough solar collector)

A model for the steam generator PTSC is developed by combining the models presented in [14], [23], [24]. In short, the model calculates the outlet steam state conditions from the water flow inlet and the external atmospheric conditions. The model includes calculations of heat losses and pressure drops along the pipe. The input parameters are the direct solar radiation, solar ray's angle of incidence, wind velocity, ambient temperature, sky temperature, the number of rows and the length. Other dimensions and optical characteristics of the unit, such as pipe aperture (w), receiver diameter (D), reflectivity and absorptance, are also included in the model. The model equally distributes the total incoming mass flow between the numbers of rows. Then, it divides the receiver into three sections depending on the water state, first and third sections are single-phase flow (liquid and steam) while the second part is two-phase flow.

The model calculates the outlet pressure by knowing the inlet pressure and pressure drop along the tubes. The pressure drops are calculated according to the single phase (heating to saturated steam and super-heating) or phase changes (evaporating) with appropriate correlations. For the single phase Darcy–Weisbach correlation is used while for the boiling section(phase changes) the Friedel correlation is used. Friedel correlation takes into account the static, momentum and friction pressure drops.

Similarly the heat flux is calculated for the three sections according to

$$Q_{absf,s} = \eta_{opt} S A_{conc,s} - U_L A_{rec,s}\left(T_{rom,s} - T_{amb}\right) \qquad s = 1,2,3 \qquad (17)$$

where $Q_{absf,s}$ is the heat absorbed by the fluid in section s, η_{opt} is the optical efficiency, $S$is the irradiation, T_{amb} is the ambient temperature, $T_{rom,s}$ is the mean temperature at the outer surface of the receiver in section s, and U_L is the mean heat transfer coefficient for the entire PTSC. The area of the concentrator in section s is defined as $A_{conc,s} = aperatur.L_s$, and similarly, the receiver area in the corresponding section is $A_{rec,s} = \pi D_{ro} L_s$. D_{ro} and L_s are the receiver outer diameter and section length respectively.

The mean heat transfer coefficient for the entire PTSC is determined using the total heat loss to the surrounding by assuming a constant mean temperature of the outer surface of the receiver and a relative coefficient of the conductive losses through the structure compared. The heat losses to the surrounding takes into account the low-pressure air conductivity, the diameters of the external surface of the receiver, the inner glass cover and external glass cover, the emissivity of the receiver, the emissivity of the glass cover, the conductivity of the glass cover, and the convection coefficient of the wind. For two-phase flow, the Gungor and Winterton is used. Basically it combines the effect of the forced convection and the nucleate boiling weighted with coefficients. Again, similar to the process of calculating the pressure drop in two-phase flow, this section is discretized into smaller segments because the heat transfer depends on the vapour quality, which varies along the pipe. Table 5. Presents the important parameter for this component assumed in this study.

Table 5. Main specifications for PTSC–SG.

PTSC	
Length	250 m
Number of rows	20
Receiver	
Diameters (D_{ri}, D_{ro})	33, 38 mm
Material	Stainless steel
Conductivity (k_r)	60 W/mK
Coating	Black Niquel
Emissivity (ε_r)	0.06
Absorptivity (α)	0.94
Cover	
Diameters (D_{ci}, D_{co})	84, 90 mm
Material	Glass
Conductivity (k_c)	0.035 W/mK
Emissivity (ε_c)	0.84
Transmissivity (τ)	0.94
Air pressure in the gap (p_m)	0.5 mbar
Concentrator	
Reflectivity (φ)	0.93
Intercept factor (γ)	0.93
Aperture	2.5 m
Incidence angle modifier (β)	1
Manifold losses	20% of the heat to ambient
Other Information	
Ambient temperature (T_{amb})	28°C
Sky temperature (T_{sky})	20°C
Wind velocity (V_{wind})	5 m/s
Saturation temperature (T_{sat})	80°C (253K)

PLANT SCHEMES

Figure 4 presents the proposed plant scheme in this study. As shown water is preheated to 430°C by the PTSC (node 3) before entering to the anode preheater. The water (now steam) is further preheated to about 660C in the anode preheated before entering the RSOC. The temperature of the off-fuel (node 6) is 750°C, which is used to preheat the steam in the anode preheater. The off-fuel after the anode preheater (node 7) is then first cooled down in a district heating heat exchanger (DH2) and then is send to a condenser for separating H2 and H2O. It shall be note that the off-fuel after the RSOC is a mixture of H2 and H2O. This mixture depends on the utilization factor of the RSOC. The higher the utilization factor, the lower the amount of water in the mixture will be.

Some of the steam after the PTSC is extracted for district heating (heat exchanger denoted as DH1 in the figure). The reason for this extraction is to regulate the temperature of steam entering the RSOC. Later on, it will be shown that the amount of this extraction is very important when wind velocity is changed. The off-air after the RSOC which is separated from the steam (node 23), has a temperature of about 750°C which can be used for different purposes such heating in the district heating (DH3) network, or cooling in the district cooling network, or water distillation for producing freshwater. Depending on the location where the plant to be installed one of these suggestions can be applied.

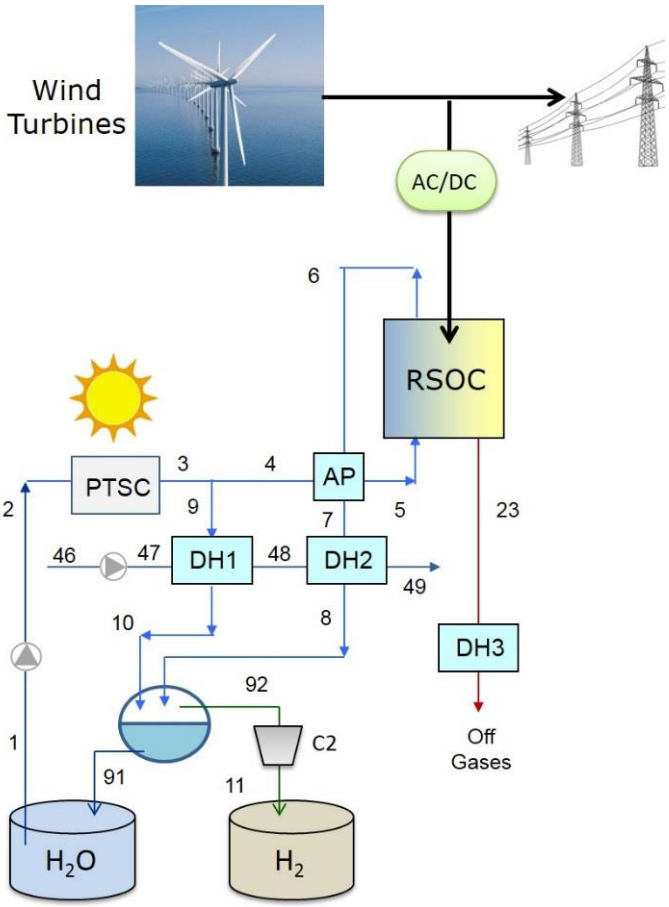

Fig. 4: Scheme of the proposed plant with district heating.
DH = district heating and AP = anode preheater.

The supply temperature for the district heating is 100°C while its return temperature is 50°C. These values are based on the current technology in Denmark. New generation district heating

under development will have supply temperature at about 50 to 60°C.

An alternative plant design in which the DH3 heat exchanger (located at the off-air side) is replaced with an absorption chiller is shown in Fig. 5. This plant is able to produce cooling (in addition to the heating) when cooling is needed, e.g. during summer time if located in colder region. Note that the DH2 can also be used for hot water production (for showering, washing, etc.). Thus, such combination provides many opportunities depending in the location.

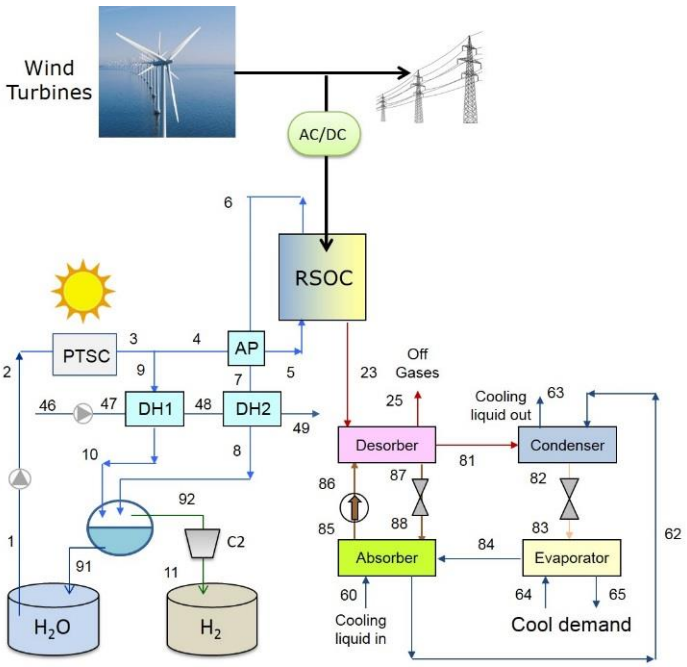

Fig. 5: Scheme of the proposed plant with district cooling.
DH = district heating and AP = anode preheater.

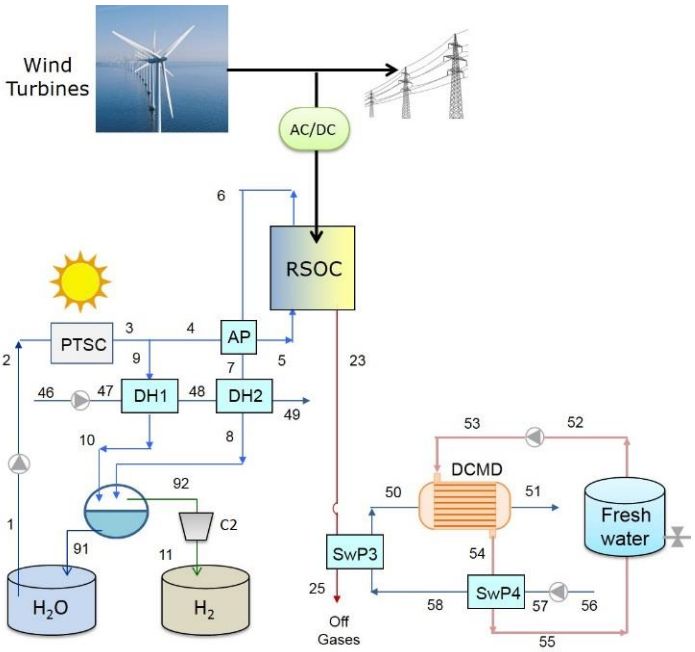

Fig. 6: Scheme of the proposed plant with freshwater production.
DH = district heating and AP = anode preheater.

A third alternative is proposed in Fig. 6, wherein the absorption chiller is replaced with a DCMD unit to produce freshwater. Freshwater getting scared in many areas and the need for such unit becomes more and more important, and therefore is studied here.

The efficiency defined above (Eq. 9) does not take account the heat production, cool production and freshwater production. It only defines fuel production. Therefore, there is a need to define a new efficiency, which accounts for other production besides the fuel production (Q_{prod}). Thus, the following efficiency is defined,

$$\eta_{plant} = \frac{\dot{m}_{H2,out} LHV_{H2} + Q_{prod}}{P_{in} + Q_{in}} \tag{18}$$

The efficiency defined above (Eq. 9) does not take account the heat production, cool production and freshwater production. It only defines fuel production. Therefore, there is a need to define a new efficiency, which accounts for other production besides the fuel production. The following equation takes also account the heat production besides the fuel production. This may be called as energy efficiency or fuel utilization efficiency.

Another point to be mentioned is that the solar energy is free and therefore one can assume that its contribution to the efficiency shall be neglected. Therefore, the following efficiencies can be defined.

$$\eta_{SOEC,2} = \frac{\dot{m}_{H2,out} LHV_{H2}}{P_{in}} \tag{19}$$

$$\eta_{plant,2} = \frac{\dot{m}_{H2,out} LHV_{H2} + Q_{prod}}{P_{in}} \tag{20}$$

Obviously, plant efficiency according to Eq. (20) may be larger than unity under certain circumstances and the reason is that it neglects the free heat input from the solar energy to the system.

RESULTS AND DISCUSSIONS

Figure 7 presents wind turbine performance curves. It shows that for any design there exists a wind velocity for which, power output is maximum (Fig. 7a).

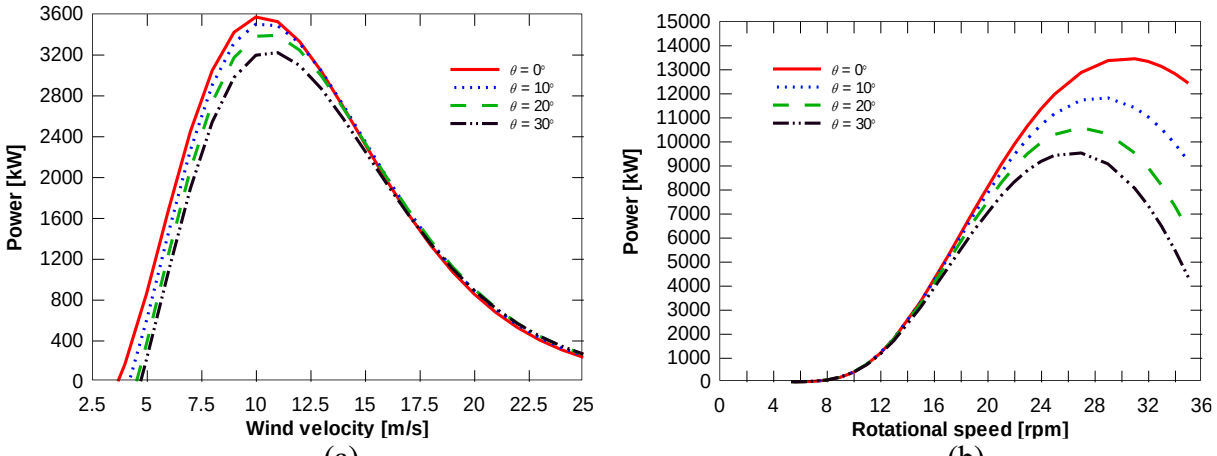

(a) (b)

Fig. 7: Wind turbine performance curves, (a) power vs wind velocity, and (b) power vs rotational speed.

It also demonstrates that for each design and at a constant wind velocity there exists a rotational speed for which turbine power is maximum (Fig. 7b). The figure also indicates that wind power decreases when wind velocity is above 12 m/s (default value for the present design). Another conclusion is that for each pitch angle there is a rotational speed at which power maximizes. This indicates that to operate the wind turbines at their peak efficiency one needs to design a variable shaft speed, but on expense of additional cost.

Plant with district heating only

As demonstrated above, one of the parameters to be studied is the wind velocity. Wind turbines electrical power strongly depends on the wind power (wind speed) which directly affects the hydrogen production through the electrolyser system. Figure 8 presents the SOEC performance when wind speed is increased. At higher wind velocities (than 12 m/s) power of the turbines decreases and thereby power feed to the electrolyser decreases. This results in lower current density while cell voltage does not change significantly. Note that RSOC stacks are run on thermos-neutral voltage (no heat supplied to the electrolyser) and therefore the changes in the cell voltage is not marked. It decreases slightly from 1.36 V to 1.32 V.

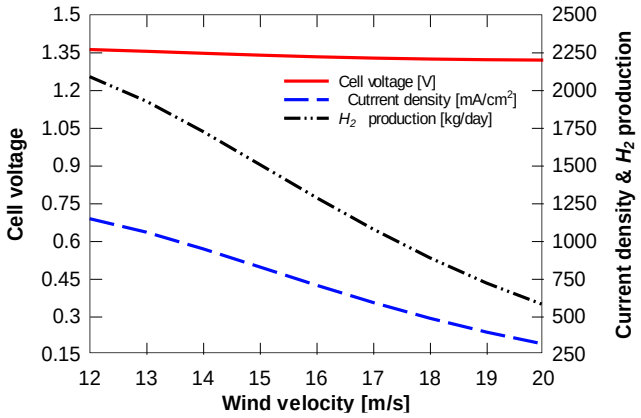

Fig. 8: SOEC performance as function of wind velocity for plant with DH connection only (c.f. Fig. 4).

Since power supplied to the electrolyser decreases then H2 production decreases as the direct result, from about 2090 kg/day to about 580 kg/day when wind velocity increases from 12 m/s to 20 m/s.

Figure 9 displays heat productions as well as heat and power consumptions by the system with district heating only. Note that Heat consumptions is coming from solar energy (PTSC) while power consumption is from wind turbines.

Heat form the solar energy through PTSC into the plant is constant since number of PTSC does not change and the temperature out of the PTSC is set to 350 °C. On the other hand, heat production for the district heating decreases significantly when wind velocity increases from 12 m/s to 20 m/s (because power from wind turbines decreases). Such decrease in heat productions is mainly due to the decrease in DH3, which is located at the off-oxygen side and depends strongly on the electrolyser performance. Heat production from DH2 located at the off-fuel side of the electrolyser decreases also as direct consequent when electricity supplied to the SOEC decreases.

However, heat produced by DH1 increases significantly when wind velocity increases. The reason is that the mass flow through the PTSC is constant (constant size and solar radiation)

while power to electrolyser decreases. Meaning that there exists excess of steam for the electrolyser and therefore this excess steam flows through DH1 instead. Consequently, DH1 produces more heat as electrolyser performance decreases. It is now obvious why the design includes a splitter after the PTSC.

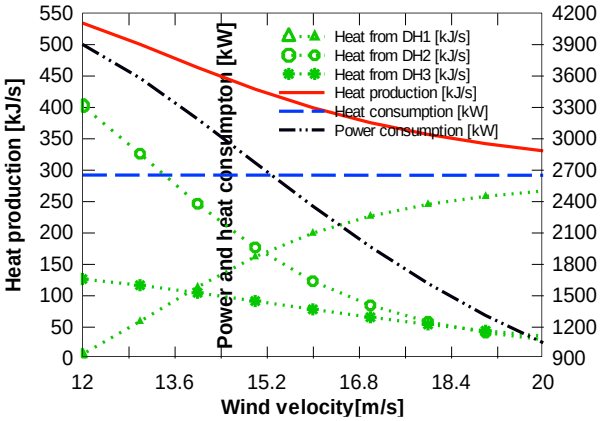

Figure 9: Heat production as function of wind velocity for plant with DH connection only (c.f. Fig. 4).

Figure 10 exhibits electrolyser system efficiency as well and as plant efficiency when heating production is included. At the design point, plant efficiency is more than 52% when heat production is included, while H2 production system efficiency is about 44%. Neglecting heat input by the solar energy (free heat) then electrolyser system efficiency is about 76% and if heat production is included then plant efficiency is close to 90%. These results are encouraging and demonstrates the importance of including renewable energy systems into current energy systems.

As mentioned above supply temperature to the district heating network is 100°C (current and mostly used technology). This indicates that some energy is lost from the system without being recovered. Decreasing DH supply temperature to 50°C (future DH generation under development) decreases energy dissipation to the environment and thereby plant efficiency increases.

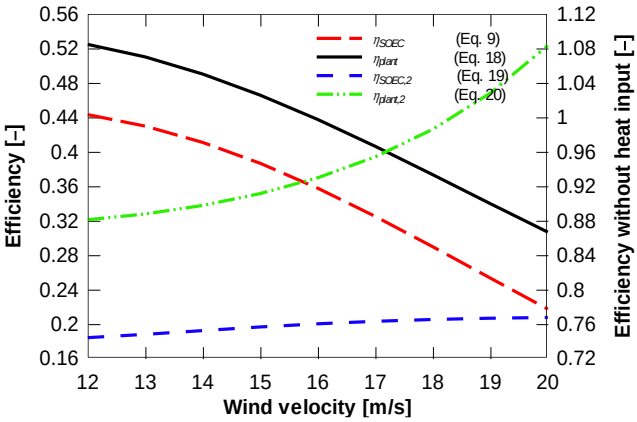

Figure 10: Plant performance as function of wind velocity for plant with DH connection only (c.f. Fig. 4).

Note that Q_{prod} in Eqs. (18) and (20) accounts for summation of all heat generated for district heating (DH1, DH2 plus DH3).

Authors from non-English speaking countries are requested to find persons who are competent in English and familiar with the scientific language who can edit their manuscripts before submission. Reviewers must not be relied upon to make corrections of English expression, spelling, etc. As there is no copy editing stage for camera-ready manuscripts, it is the responsibility of authors to ensure that the presentation of their papers reaches the same high level as that of the work they describe.

Plant with district heating and cooling

The results for the plant with both DH and absorption chiller is revealed in Fig. 11. Off-air after the desorber is dissipated at 90°C, well above the dew point. Now, Q_{prod} in Eqs. (18) and (20) accounts for summation of heat and cool generation. Multiplying the mass flow of the cooling flow with the enthalpy difference over the evaporator, calculates the generated cooling effect.

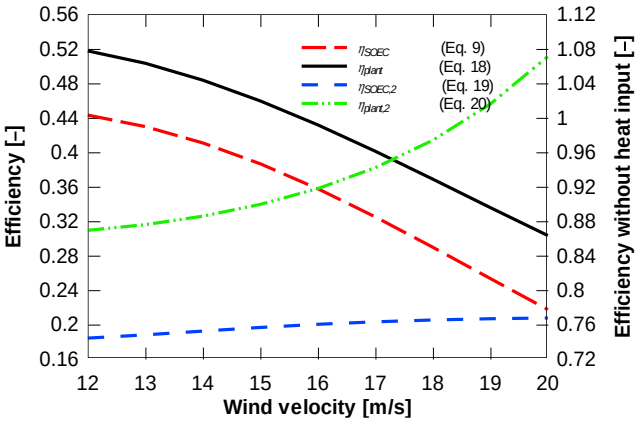

Figure 11: Plant performance as function of wind velocity for plant with DH connection and AP (c.f. Fig. 5).

The results obtained here are very similar to the previous case. SOEC system and plant efficiencies decreases with increasing wind velocity (due to less power generated by the turbines) while the alternative efficiencies (neglecting solar heat input) increases with wind velocity. Again, identifying that polygeneration systems are benefitting when combining with renewable sources.

Plant with district heating and freshwater

Figure 12 demonstrates the results obtained here from the plant which generates both heat and freshwater in addition to the hydrogen production (c.f. Fig. 6).

Again the results are similar as the previous case, signifying that the definition in Eqs. (18) and (20) can be used for all polygeneration systems.

In this case, Q_{prod} in Eqs. (18) and (20) is the summation of heat and freshwater generation. Multiplying the mass flow of the freshwater with the enthalpy difference over the DCMD at freshwater side, calculates the generated freshwater effect, which would be comparable with hydrogen production.

As noted, that the efficiency according to Eq. (20) is slightly larger than 100% because this equation neglects the heat added to system from the solar energy. Including this heat, the plant efficiency will be slightly larger than 52%.

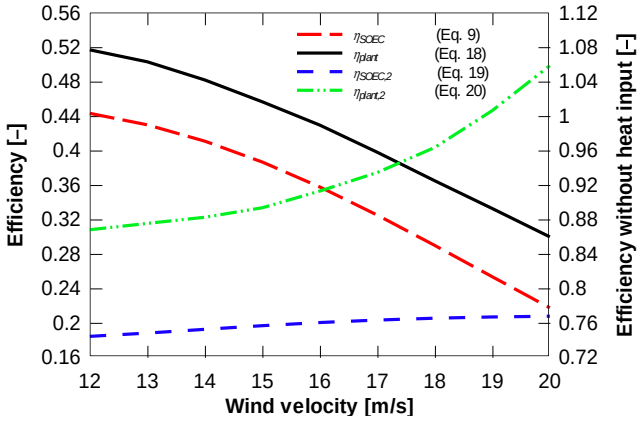

Figure 12: Plant performance as function of wind velocity for plant with DH connection and DCMD (c.f. Fig. 6).

Finally, the performance of the absorption chiller is calculated to be 0.617, which is the ratio between the heat released in the evaporator (cooling effect) over the heat absorbed in the desorber. The performance of the DCMD is calculated to be 0.934, which is the ratio between the heat absorbed by the freshwater, and the heat lost by the seawater in the DCMD.

As shown above, large wind velocity affect significantly on plant performances while small changes in wind velocity may have minor effect on plant performance. Solar radiation changes significantly during a day and therefore, it has some effect on plant performances. Therefore, a dynamic model may better capture plant performance by knowing solar radiation and wind velocity hour per hour for a specified location. Such data are usually available from the weather data for the region where the plant is placed.

CONCLUSION

A polygeneration system based on reversible solid oxide cells is presented and analysed for hydrogen, heat, cool and freshwater production.

Analysis shows that the RSOC system efficiency reaches to about 44% when only hydrogen production is accounted (also the main aim). Accounting other productions (heat, cool and freshwater) increases plant efficiency to about 75%.

Neglecting heat input to the system through solar energy increases RSOC efficiency to about 52% (hydrogen production only) and accounting for all productions (hydrogen, heat and cooling), the plant efficiency reaches to about 90%.

NOMENCLATURE

A : Area (m2)
E : Voltage (V)
J : Current (Amp)
$\dot{m}$: Mass flow (kg.s–1)
N : Number (–)
P : Power (W)
p : Pressure (N.m–2)
Q : Heatr (W)
S : Swept area (m2)
U : Heat transfer coefficient (W.m–2)

W : Work (W)
w : Angular rotation (rad.s–1)
Greek letters
η : Efficiency (–)
λ : Tip speed ratio (rad)
ρ : Density (kg.s–1)
Abbreviation
DCMD : Direct contact membrane distillation
RSOC : Reversible solid oxide cell
Subscripts
amb : Ambient
act : Activation
cons : Concentration
ohm : Ohmic
prod : Production
rom : mean at the outer surface
SOEC : Solid oxide electrolyse cell

REFERENCES

1. Ni M, Leung MKH, Leung DYC, Technological development of hydrogen production by solid oxide electrolyzer cell (SOEC). Hydrogen Energy, 33, 2337–2354 (2008).
2. Abuadala A, Dincer I, Exergoeconomic analysis of a hybrid system based on steam biomass gasification products for hydrogen production. Hydrogen Energy, 36, 12780–12793 (2001).
3. Viviani M, Canu G, Carpanese MP, Barbucci A, et al. Dual cells with mixed protonic-anionic conductivity for reversible SOFC/SOEC operation. Energy Procedia, 2, 182–189 (2012).
4. Dillig M, Leimert J, Karl J. Planar High Temperature Heat Pipes for SOFC/SOEC Stack Applications. Fuel Cells, 14, 479–488 (2014).
5. Burgoyne A, Vahdati MM. Direct Contact Membrane Distillation. Desalination and Water Treatment, 35(8), 1257–1284 (2000).
6. Shirazi MMA, Kargari A, Shirazi MJA. Direct contact membrane distillation for seawater desalination. Separation Science and Technology, 49, 368–375 (2012).
7. Suárez F, Ruskowitz JA, Tyler SW, Childress AE. Renewable water: Direct contact membrane distillation coupled with solar ponds. Applied Energy, 158, 532–539 (2015).
8. Nakoa K, Date A, Akbarzadeh A. DCMD modelling and experimental study using PTFE membrane. Desalination and Water Treatment, 57, 3835–3845 (2016).
9. Cath TY, Adams VD, Childress AE. Experimental study of desalination using direct contact membrane distillation: a new approach to flux enhancement. Membrane Science, 228, 5–16 (2003).
10. Akikur RK, Saidur R, Ping HW, Ullah KR. Performance analysis of a co-generation system using solar energy and SOFC technology. Energy Conversion and Management, 79, 415–430 (2014).
11. Ni M, Leung KH, Leung DYC. Energy and exergy analysis of hydrogen production by solid oxide steam electrolyzer plant. Hydrogen Energy, 32, 4648–4660 (2007).
12. Rokni M. Thermodynamic analyses of municipal solid waste gasification plant integrated with solid oxide fuel cell and Stirling hybrid system. Hydrogen Energy, 40, 7855–7869 (2015).
13. Hernández-Pacheco E, Singh D, Nutton PN, Patel N, Mann MD. A macro-level model for determining the performance characteristics of solid oxide fuel cells. Power Sources, 138, 174–186 (2004).
14. Duffie JA and Beckman WA. *Solar Engineering of Thermal Processes*. 4th Ed., John Wiley& Sons, 2013, ISBN 978-1-118-41541-2 (ebk).

15. Nellis G, Klein S. *Heat Transfer*. Cambridge 2009, ISBN 978-0-521-88107-4.
16. Kim YD, Thu K, Ghaffour N, Ng KC. Performance investigation of a solar-assisted direct contact membrane. Membrane Science, 427, 345–364 (2013).
17. Franchinia G, Notarbartolo E, Padovan LE, Perdichizzi A. Modeling, Design and Construction of a Micro-scale Absorption Chiller. Energy Procedia, 82, 577–583 (2015).
18. de Vega M, Almendros-Ibanez JA, Ruiz G. Performance of a LiBr–water absorption chiller operating with plate heat exchangers. Energy Conversion and Management, 47, 3393–3407. (2006).
19. Porumb R, Porumb B, Balan M. Numerical investigation on solar absorption chiller with LiBr-H2O operating conditions and performances. Energy Procedia, 112, 108–117 (2017).
20. Misra RD, Sahoo PK, Gupta A. Thermoeconomic Optimization of a LiBr/H2O Absorption Chiller Using Structural Method. Energy Resources Technology, 127, 119–124 (2005).
21. Patek J, Klomfar JA. Computationally effective formulation of the thermodynamic properties of LiBr-H2O solutions from 273 to 500 K over full composition range. Int. J. of Refrigeration, 29(4), 566–78 (2006).
22. Manyonge AW, Ochieng R, Onyango F, Shichikha J. Mathematical modelling of wind turbine in a wind energy conversion system: Power coefficient analysis. Applied mathematical sciences, 6(91), 4527–4536 (2012).
23. Odeh SD, Morrison GL and Behnia M. Modeling of parabolic trough direct steam generation solar collectors. Solar Energy, 62, 395–406 (1998).
24. Gungor KE, Winteron RHS. A general correlation for flow boiling in tubes and annuli. Int. J. Heat Mass Transfer, 29(3), 351–358 (1986).